Supplementary Information

Fano resonant $Ge_2Sb_2Te_5$ nanoparticles realize switchable lateral optical force

Tun Cao*,Libang Mao,Dongliang Gao,Weiqiang Ding,and Cheng-Wei Qiu*

*E-mail: caotun1806@dlut.edu.cn&eleqc@nus.edu.sg

S1. Absorption cross section C_{abs} of the phase-change particles in both amorphous and crystalline states.

The scattering and extinction cross sections of the phase-change nanosphere can be computed from eqn (s1) and (s2), respectively [54]:

$$C_{sca} = \frac{\lambda^2}{\pi}\sum_{n=1}^{\infty}\sum_{m=-n}^{+n}\frac{2n+1}{n(n+1)}\frac{(n+|m|)!}{(n-|m|)!}(|a_n|^2|g_{n,TM}^m|^2+|b_n|^2|g_{n,TE}^m|^2) \quad \text{(s1)}$$

$$C_{ext} = \frac{\lambda^2}{\pi}\mathrm{Re}[\sum_{n=1}^{\infty}\sum_{m=-n}^{+n}\frac{2n+1}{n(n+1)}\frac{(n+|m|)!}{(n-|m|)!}(a_n|g_{n,TM}^m|^2+b_n|g_{n,TE}^m|^2)] \quad \text{(s2)}$$

where C_{sca} is scattering cross section and C_{ext} extinction cross section, and the absorption cross section C_{abs} of the particle is given by eqn (s3).

$$C_{abs} = C_{ext} - C_{sca} \quad \text{(s3)}$$

Figure S1 shows the peak of C_{abs} shifts towards the shorter wavelength (from 660 to 600nm) when the phase of $Ge_2Sb_2Te_5$ switches from amorphous to crystalline. However, a difference of the C_{abs} between the amorphous and crystalline particle is not large around λ= 640 nm, where C_{abs}=2.2x10^{-13} m^2 for the amorphous and C_{abs} = 1.4x10^{-13} m^2 for the crystalline. This indicates a small difference in the absorptivity of the phase-change particles in amorphous and crystalline states. Moreover, the phase-change nanoparticles are manipulated by a Gaussian pulse with a very low power intensity (~10 mW/μm^2) and have the cooling effect owing to the convection in the aqueous environment. Therefore, herein the optical heating may not significantly disturb the optical parameters of the phase-change particles.

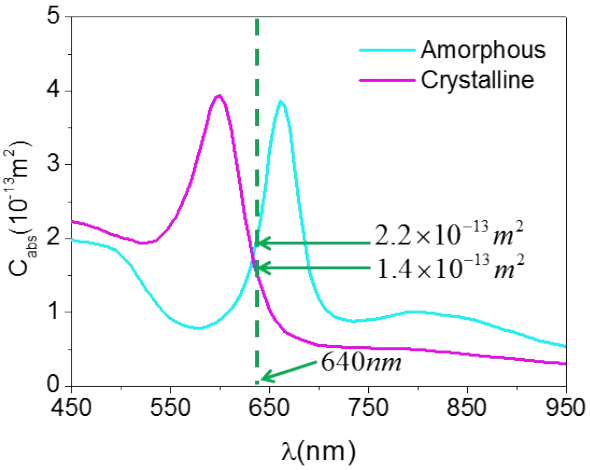

Fig. S1 Absorption cross section C_{abs} for the crystalline (shown by the pink solid line) and amorphous nanoparticle (shown by the cyan solid line). The nanoparticles are in the water environment.

S2. Optimization of the radius of $Ge_2Sb_2Te_5$ core (R_{PCM}) and thethickness of Au shell (T_{Au}).

The total lateral force F_x originating from the dipole-quadrupole Fano resonance (DQ-FR) closely relates to the thickness of the Au shell (T_{Au}) owing to the strong coupling between the outer and inner surface of the shell. In Fig.S2, we investigate the F_x acted on the phase-change nanoparticles with Au shell (thickness T_{Au}= 10,20,30 and 40 nm) and crystalline $Ge_2Sb_2Te_5$ core (R_{PCM}=70nm), where the particles located at half waist of the Gaussian beam ($x = w_0/2$). As can be seen, the dip of F_x induced by the DQ-FR appears at λ = 688, 620, 618, and 632 nm for T_{Au}= 10, 20, 30, and 40 nm, accordingly. Quality (Q) factor is defined by the resonant frequency (ω_0) over the line-width of the autoionized states (γ), where ω_0 and γ are obtained from Fano formula (eqn (1)) by fitting F_x curves shown in Fig.S2. The fitting parameters are presented in Table S1.

$$I_{\text{Fano}} = I_0 \frac{1}{1+\Gamma^2}\frac{(\Gamma\gamma+\omega-\omega_0)}{(\omega-\omega_0)^2+\gamma^2}+I_b \qquad (1)$$

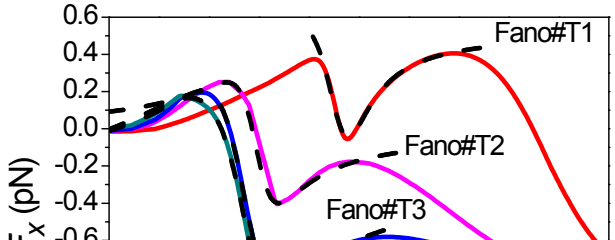

Fig. S2 Fano fitting on the F_x spectra for the crystalline particle with various Au shell thicknesses (T_{Au}= 10,20,30 and 40 nm) and a fixed radius of crystalline $Ge_2Sb_2Te_5$ core (R_{PCM}=70nm).

In Table S1, it can be seen that Q factor of the DQ-FR induced F_x reduces with increasing T_{Au}. The sharpest resonant dip of the F_x curve is observed at λ = 688 nm for T_{Au}= 10 nm, where γ is 1.05x10^{14} rad/s, and Q factor 26.38. However, considering its practical application, here we choose T_{Au}= 20 nm exhibiting the second strongest Q factor of 23.26 since its resonant wavelength of the DQ-FR (λ = 620 nm) is close to the commonly used laser: λ = 633 nm.

Table S1. Parameters used in the FR line shape to fit the F_x spectra for phase-change nanoparticle with Au shell (thickness T_{Au}= 10,20,30 and 40 nm) and crystalline $Ge_2Sb_2Te_5$ core (R_{PCM}=70nm).

Lable	ω_0	γ	Γ	I_0	I_b	Q
Fano #T1	2.77×10^{15}	1.05×10^{14}	0.3354	0.6499	-0.04242	26.38
Fano #T2	3.14×10^{15}	1.35×10^{14}	0.75	0.65	–0.4	23.26
Fano #T3	3.21×10^{15}	2.1×10^{14}	-1.228	-1.039	0.2035	15.3
Fano #T4	3.17×10^{15}	2.74×10^{14}	-1.388	-1.352	0.1659	11.57

Figure S3 shows the comparison of F_x between the amorphous and crystalline nanoparticles located at $x = w_0/2$ for various core radius R_{PCM}=50,60,70 and 80 nm with a fixed Au shell thickness of T_{Au}= 20 nm. The switchable feature of F_x becomes more significant as increasing R_{PCM}. Figure S3(d) shows the F_x can obtain the highest transition from +0.27 to –0.56 pN for R_{PCM}= 80 nm at $\boldsymbol{\lambda}$ = 680 nm. However, this transition appearing at $\boldsymbol{\lambda}$ = 680 nm is beyond the spectra of the commonly used laser ($\boldsymbol{\lambda}$ = 633 nm). In terms of the experimental realization, we optimized the radius of $Ge_2Sb_2Te_5$ core at R_{PCM}= 70 nm which possesses the largest transition of F_x (from +0.14 to –0.34 pN) at $\boldsymbol{\lambda}$ = 640 nm.

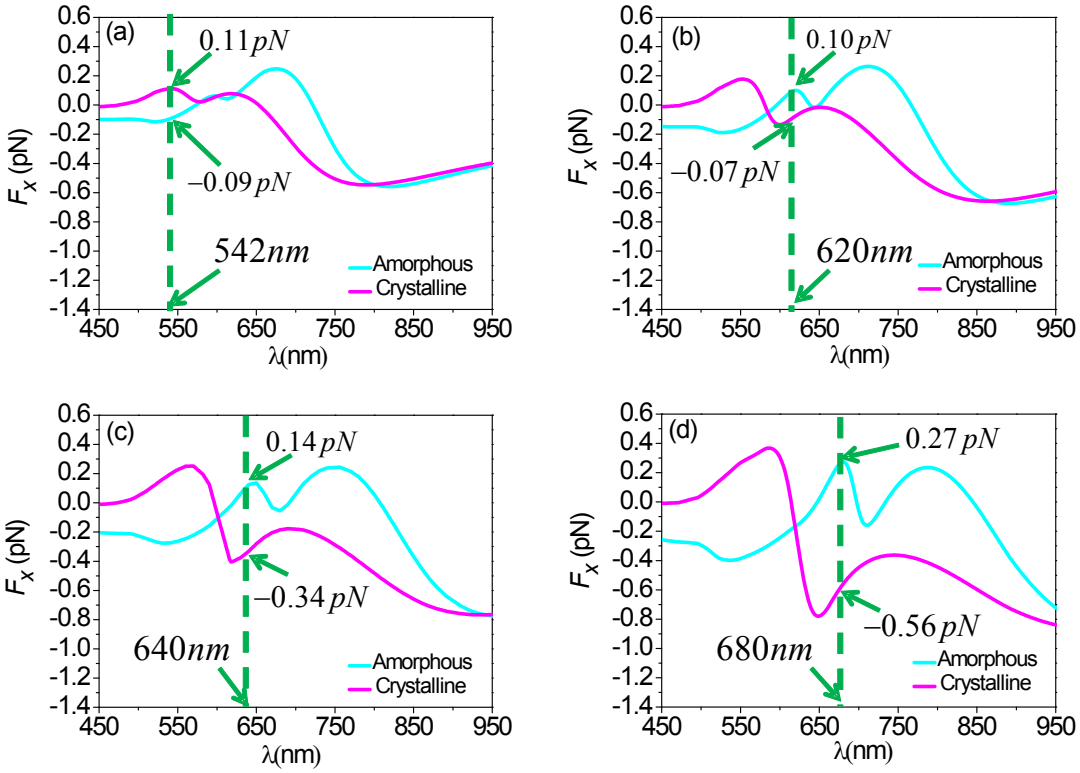

Fig. S3 F_x for both the crystalline nanoparticle shown by the pink solid line and amorphous nanoparticle shown by the cyan solid line with (a) R_{PCM}=50 nm, (b) R_{PCM}=60 nm, (c) R_{PCM}= 70 nm, (d) R_{PCM}= 80 nm, where the Au shell thickness is fixed at T_{Au}= 20 nm and the nanoparticles are both bonded by PSS in the water environment.

S3. Dynamical simulation of stability for the phase-change particle under lateral optical force.

For the phase-change particles with random Brownian motion in aqueous environment, it is necessary to analyse its stability. The phase-change particle's motion is modeled by the Langevin equation [60-61]

$$\frac{d^2x(t)}{dt^2} = -\frac{\beta}{m}\frac{dx(t)}{dt} + \frac{\zeta}{m}W_x(t) + \frac{F_x(x,y)}{m} \tag{s4}$$

$$\frac{d^2y(t)}{dt^2} = -\frac{\beta}{m}\frac{dy(t)}{dt} + \frac{\zeta}{m}W_y(t) + \frac{F_y(x,y)}{m} \tag{s5}$$

where $x(t)$ and $y(t)$ are the particle's positions, $F_x(x,y)$ and $F_y(x,y)$ are the lateral forces, $W_x(t)$ and $W_y(t)$ are the stochastic noise terms that model random collisions from fluid molecules along both the x-axis and y-axis respectively, m the mass of the spheres, $\beta = 6\pi\eta(R_{PCM} + T_{Au})$ the drag coefficient (from Stoke's law for a spherical particle), $\eta = 0.89mPa \cdot s$ the viscosity of water. The scaling constant for the stochastic noise term is given by $\zeta = \sqrt{2\beta k_B T}$ where k_B is Boltzmann's constant and $T = 300K$. The simulation algorithm was run for a total of 2500 000 time-steps with a very short time-step of 1 ns.

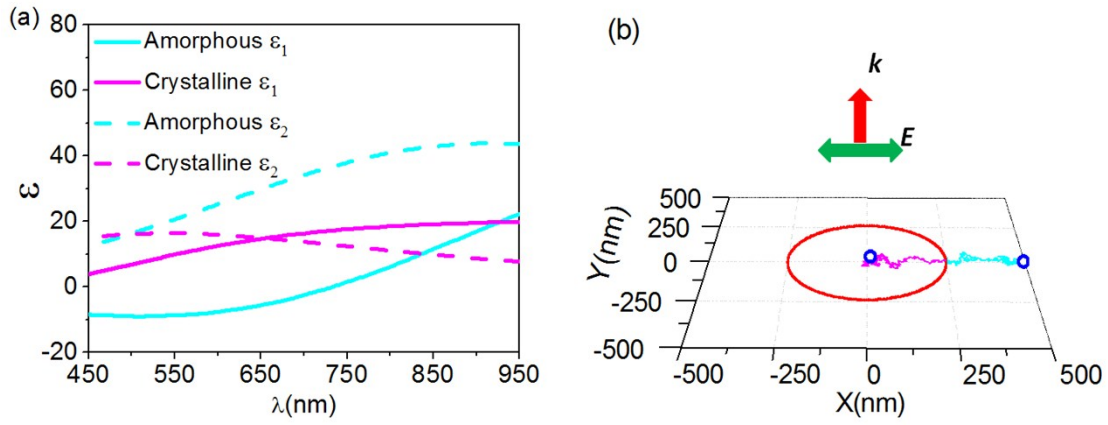

Fig. S4 (a) Dielectric constant $\varepsilon_1(\omega)$ and $\varepsilon_2(\omega)$ vs wavelength for both amorphous and

crystalline phases of $Ge_2Sb_2Te_5$.(b) Observations of stability for the phase-change particle under lateral optical force. The pink and cyan solid lines present the 2.5 ms trajectories of the crystalline and amorphous spheres of R_{PCM}= 70 nm and T_{Au}= 20 nm, accordingly. The particles are illuminated by a Gaussian beam with a low incident power P_0 = 10 mW. The ends of trajectories are indicated by small blue circles and the red solid ring denotes the illumination spot of the Gaussian beam in the focal plane (z = 0 plane).The wave vector and polarization are indicated by red and green arrows. The spheres are initially placed off-axis in a Gaussian beam ($x = w_0/2$ = 250 nm) and bonded by PSS in the water environment.

The real, $\varepsilon_1(\omega)$ and imaginary, $\varepsilon_2(\omega)$ parts of the dielectric function for the different states of $Ge_2Sb_2Te_5$were obtained from the published Fourier transform infrared spectroscopy data in [45], which for the visible spectral range are shown in Fig. S4(a). In Fig.S4 (b), we dynamically simulated the stability of the nanoparticles by observing time sequences of the movements of phase-change spheres (R_{PCM} =70nm, T_{Au} =20nm) for amorphous and crystalline states in the focal plane of the Gaussian beam (z = 0 plane), where the particle in two dimensions (x-y plane) is tracked with nanometer precision. The beam waist of the Gaussian beam is w_0 = 500nm and the power of the beam is P_0 =10 mW. Both of the situations are excited at λ= 640 nm. A 2.5 ms trajectory of the crystalline sphere is shown in the pink solid line. Owing to the excitation of the DQ-FR, a lateral scattering force (^sF_x) is generated along the $-x$ axis (see Fig. 2(d)) and, combined with the gradient force (F_{grad}) towards the center of the Gaussian source, this results in a negative F_x and thus causes a motion of the crystalline particle to the center of the incident light (Supplementary Movie_S1_crystalline). In contrast, within illumination by the Gaussian beam, the amorphous nanoparticle follows opposite direction of motion (see cyan solid line). This is due to the asymmetrical scattering in the x-z plane (see Fig. 2(c)), where the ^sF_x generated along the $+x$ axis is larger than the F_{grad} hence pushing the amorphous particle away the beam center (Supplementary Movie Movie_S2_amorphous). As can be seen in both Fig.S4(b) and supplementary movies, the phase-change nanoparticles only thermally fluctuate from -58 to 51 nm for the crystalline and from -35 to 60 nm for the amorphous along the *y-axis*, which would not significantly affect the lateral sorting of the spheres along the *x-axis*.

[45] K. Shportko, S. Kremers, M. Woda, D. Lencer, J. Robertson, and M. Wuttig, *Nat. Mater*., 2008,**7**, 653-658.

[54] G. Gouesbet, B. Maheu, and G. Grehan, *J. Opt. Soc. Am. A*, 1988,**5**, 1427-1443.

[60] P. Langevin,*C. R.Acad. Sci. Paris*, 1908,**146**, 530.

[61] P.Hansen, Y. Zheng, J. Ryan, and L. Hesselink, *Nano Lett.*, 2014,**14**, 2965.